Multi-Enzyme Nanozyme Targeting Redox-Senescence-Angiogenesis Axis Ameliorates Pathological Angiogenesis in Retinopathy Models

Authors:

Shuo-Shuo Gu,[a,b] Ling-Xiao Xia,[a,b] Yi-Peng Li,[a,b] Jian-Ying Chen,[a,b] Ya-Ni Wu,[a,b] Yu-Hong Cui,[c,d] Huai-Jie Huang,[e*] Jing Meng,[b,e**] Qingsong Mei,[f***] Hong-Wei Pan,[a,b****]

[a]Institute of Ophthalmology, School of Medicine, Jinan University, Guangzhou, Guangdong 510632, China

[b]Department of Ophthalmology, the First Affiliated Hospital, Jinan University, Guangzhou, Guangdong 510632, China

[c]Department of Cardiology, Guangzhou Institute of Cardiovascular Disease, Guangdong Key Laboratory of Vascular Diseases, The Second Affiliated Hospital, Guangzhou Medical University, Guangzhou, Guangdong 510260, China

[d]Department of Histology and Embryology, School of Basic Medical Sciences, Guangzhou Medical University, Guangzhou, Guangdong 510182, China

[e]Department of Ophthalmology, The Affiliated Shunde Hospital of Jinan University, Foshan, Guangdong 528000, China

[f]Department of Medical Biochemistry and Molecular Biology, School of Medicine, Jinan University, Guangzhou, Guangdong 510632, China

Corresponding Authors

[****] Institute of Ophthalmology, School of Medicine, Jinan University, 601 West Huangpu Avenue, Guangzhou, Guangdong 510632, China; Department of Ophthalmology, the First Affiliated

Hospital, Jinan University, Guangzhou, Guangdong 510632, China; Email: pan_hongwei@163.com

*** Department of Medical Biochemistry and Molecular Biology, School of Medicine, Jinan University, Guangzhou, Guangdong 510632, China; Email: qsmei@jnu.edu.cn

** Department of Ophthalmology, the First Affiliated Hospital, Jinan University, Guangzhou, Guangdong 510632, China; Department of Ophthalmology, The Affiliated Shunde Hospital of Jinan University, Foshan, Guangdong 528000, China; Email: 37970860@qq.com

* Department of Ophthalmology, the Affiliated Shunde Hospital of Jinan University, Foshan, Guangdong 528000, China; Email: Sally20052005@163.com

Methods:

1. CAT activity

To evaluate the CAT-like activity of PBzyme, different concentrations of PBzyme (0–50 μg/mL) were incubated with 0.8 M H_2O_2, and dissolved oxygen levels were continuously monitored for 20 min at fixed time intervals using a dissolved oxygen meter (JPSJ-606L, Leici, China). For kinetic analysis, varying concentrations of H_2O_2 (0–0.8 M) were mixed with PBzyme (12.5 or 25 μg/mL), and the amount of oxygen generated within the first 5 min was recorded to calculate the initial reaction rates, thereby assessing the catalytic efficiency of PBzyme toward H_2O_2 decomposition.

2. ICP

For biodistribution analysis, mice were intraperitoneally injected with PBzyme at a dose of 20 mg/kg based on body weight. At 12 h post-injection, the animals were euthanized, and retinas from

both control and PBzyme-treated groups were carefully harvested. The tissues were dried, weighed, and subsequently digested in nitric acid (HNO_3, 1% in deionized water) until complete dissolution. The resulting solutions were filtered and analyzed by inductively coupled plasma mass spectrometry (ICP, Thermo iCAP 700 series).

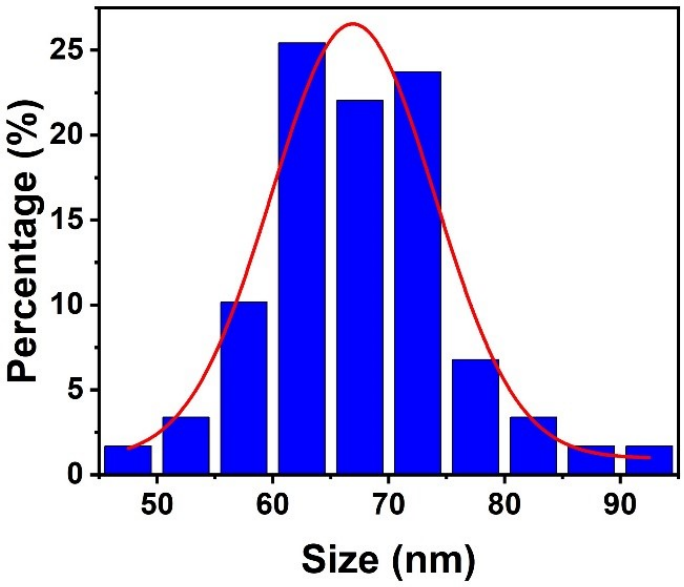

Fig. S1. Size distribution analysis of PBzyme based on TEM images. Histogram showing the particle diameter distribution (count ≥ 100 nanoparticles). The average size is approximately 70 nm.

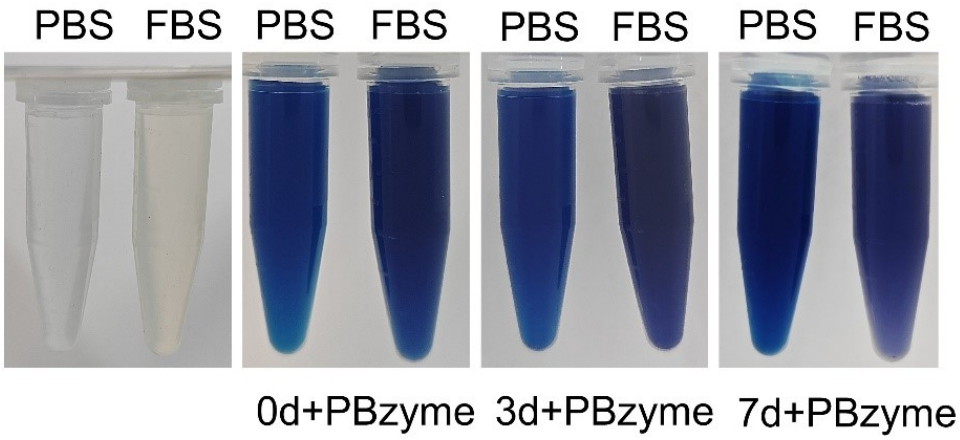

Fig. S2. Stability of PBzyme in physiological media. Photographs of PBzyme dispersions in phosphate-buffered saline (PBS, pH 7.4) and fetal bovine serum (FBS) at days 0, 3, and 7. No visible aggregation or precipitation was observed.

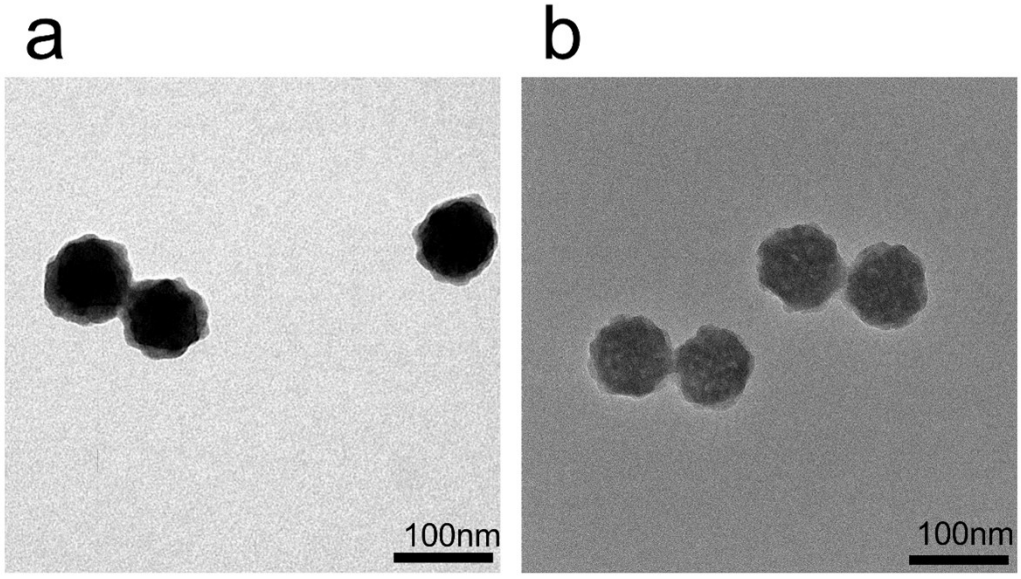

Fig. S3. TEM analysis of PBzyme stability in serum. TEM images of PBzyme nanoparticles before (left) and after (right) incubation in FBS at 37°C for 7 days. Scale bar: 100 nm.

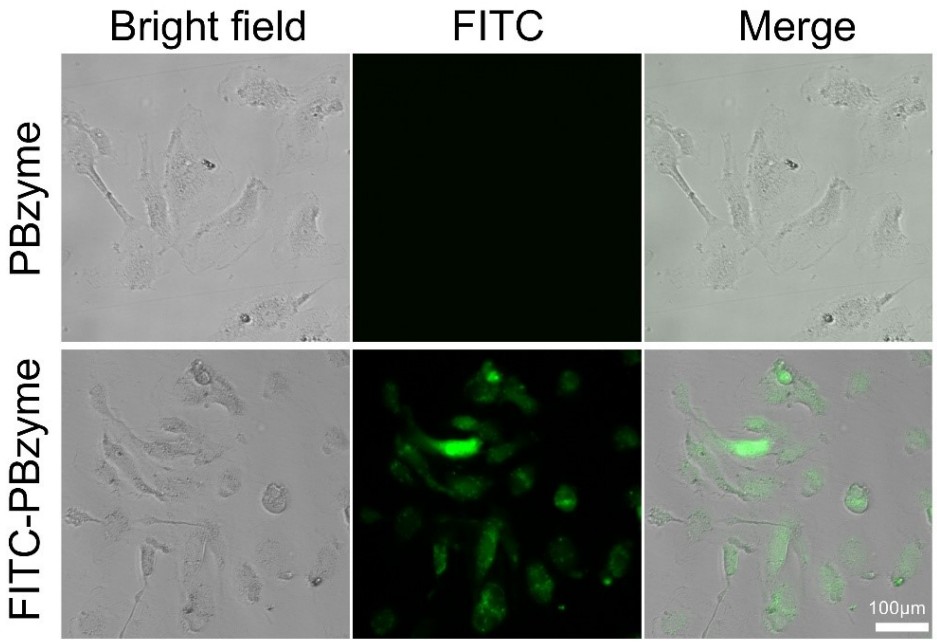

Fig. S4. Cellular Uptake of PBzyme. Bright-field and FITC fluorescence images of PBzyme were acquired. Following FITC labeling and a 4-hour co-culture with cells, high fluorescence intensity was observed inside the cells, indicating the internalization of PBzyme. Scale bar: 100μm.

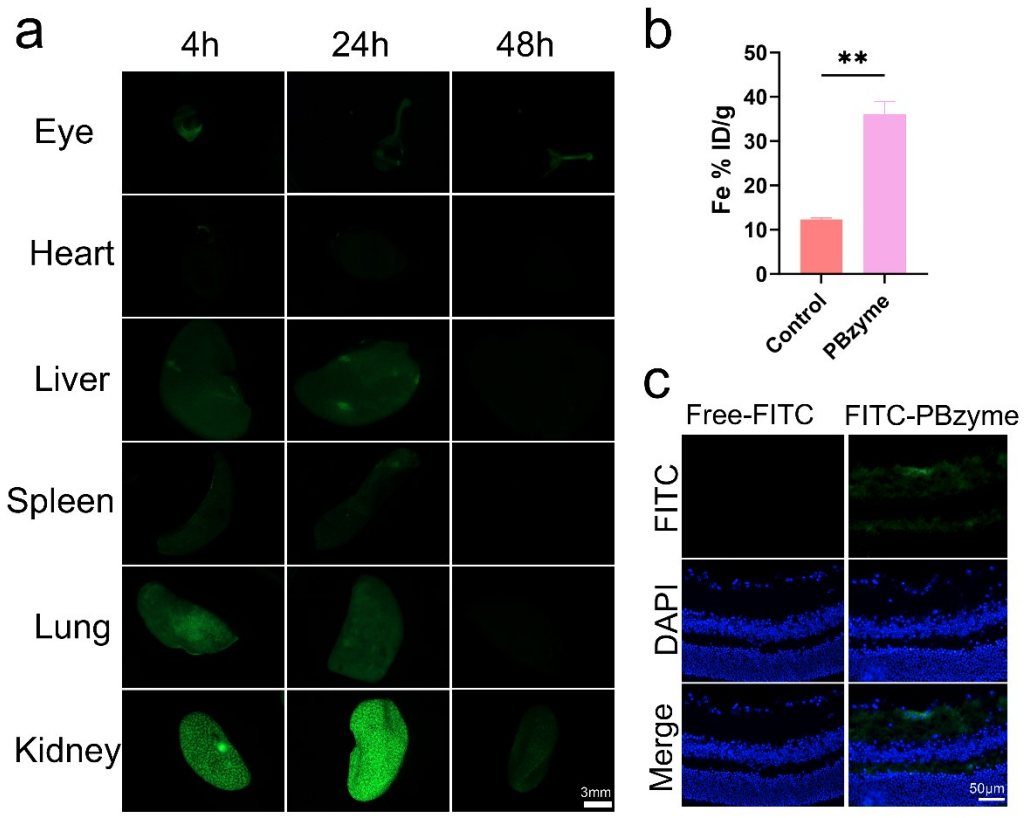

Fig. S5. In Vivo Distribution of PBzyme. (a) The fluorescence intensity in the eye, heart, liver, spleen, lung, and kidney after intraperitoneal injection of PBzyme at 4h, 24h and 48h. (b) Iron (Fe) concentrations in retinal tissues from different groups 12 h after intraperitoneal administration of PBzyme (20 mg/kg). (c) Immunofluorescence images of retinal sections following intraperitoneal administration of FITC-labeled PBzyme. FITC signals (green) indicate PBzyme distribution, and nuclei were counterstained with DAPI (blue). Scale bar: a, 3mm. c, 50μm, (n = 3, $^{**}P < 0.01$).

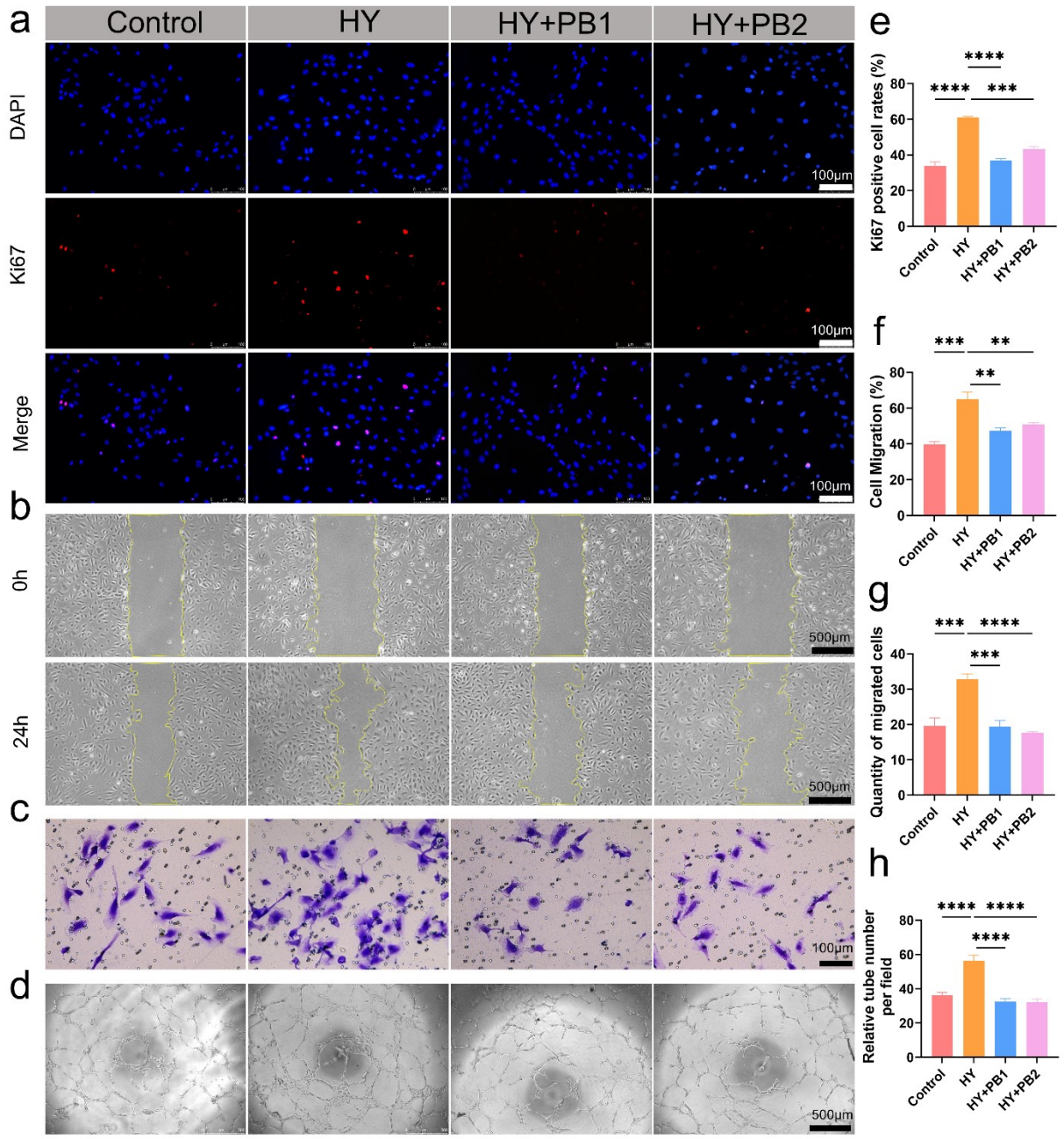

Fig. S6. PBzyme suppresses hypoxia-induced hyperactivation of endothelial cells. HRMECs were treated under hypoxia (HY, 1% O_2) with or without PBzyme (PB1, PB2). Analyses parallel to those in Fig. 5: (a) Ki67 staining; (b) Wound healing; (c) Transwell migration; (d) Tube formation. (e-h)

Corresponding quantifications. Scale bars: a, 100 μm; b, d, 500 μm; c, 100 μm. (n = 3; $^{**}P < 0.01$, $^{***}P < 0.001$, and $^{****}P < 0.0001$).

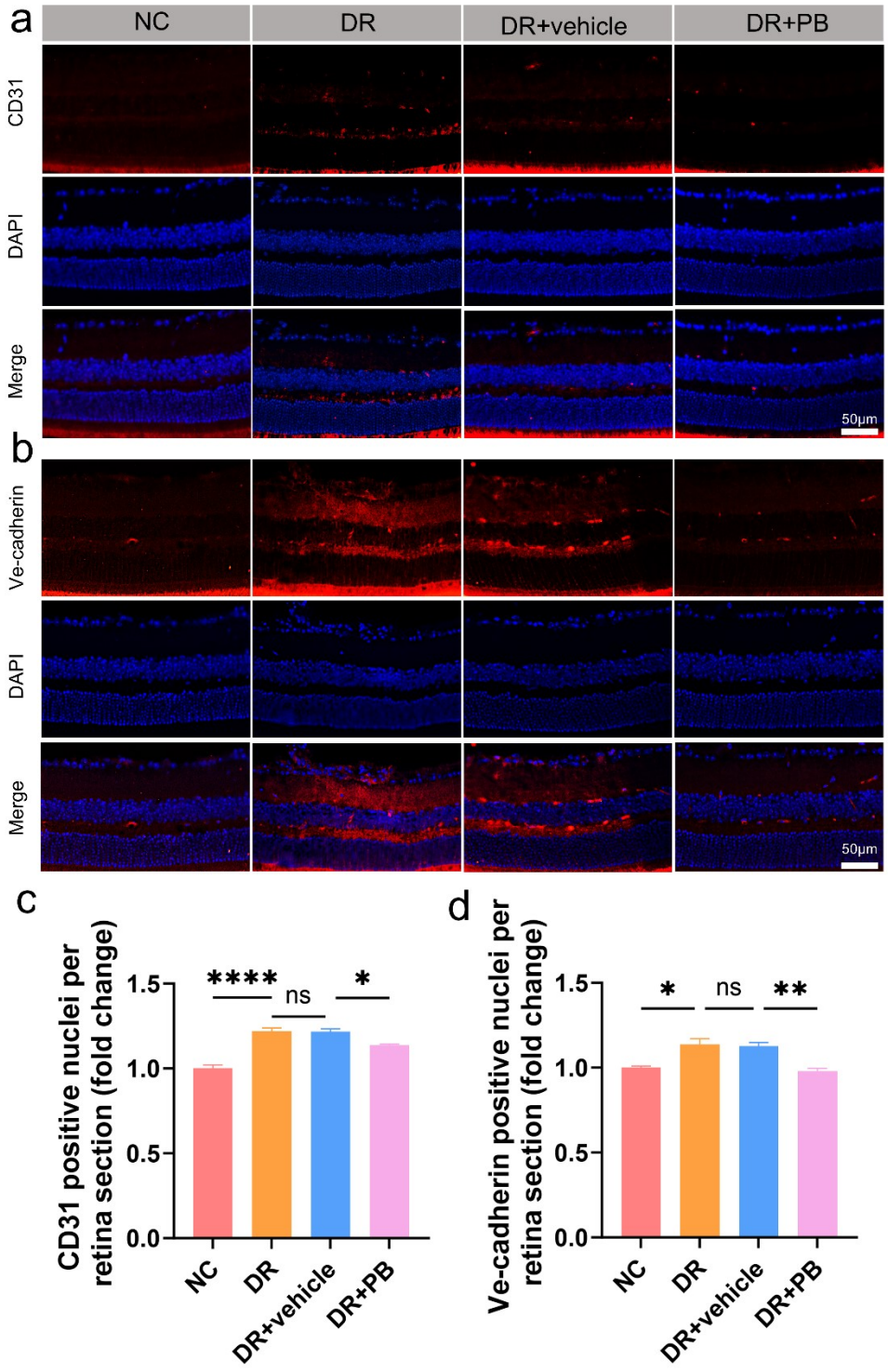

Fig. S7. PBzyme downregulates angiogenic marker expression in diabetic retinas. (a, b)

Representative immunofluorescence images of retinal sections stained for CD31 (a) and VE-cadherin (b) (red). Nuclei are counterstained with DAPI (blue). Scale bar: 50 μm. (c, d) Quantitative analysis of mean fluorescence intensity for CD31 (c) and VE-cadherin (d). (n=6, $*P < 0.05$, $**P < 0.01$, $****P < 0.0001$, ns: not significantly different).

Supplementary Table

Table S1

Primer sequences for RT-qPCR.

Gene	Forward (5'-3'sequence)	Reverse (5'-3'sequence)
IL-6	CATCCTCGACGGCATCTCAG	TCACCAGGCAAGTCTCCTCA
IL-1β	CTCTCTCCTTTCAGGGCCAA	GCGGTTGCTCATCAGAATGT
TNF-α	GCCCATGTTGTAGCAAACCC	TGAGGTACAGGCCCTCTGAT
MCP-1	CACCAATAGGAAGATCTCAGTGC	TGAGTGTTCAAGTCTTCGGAGTT
CCL-5	TACACCAGTGGCAAGTGCTC	CATCCTTGACCTGTGGACGA
GADPH	CAAATTCCATGGCACCGTCA	GACTCCACGACGTACTCAGC